

Fully Integrated Patch Based on Lamellar Porous Film Assisted GaN Optopairs for Wireless Intelligent Respiratory Monitoring

Zecong Liu,[†] Junjie Su,[†] Kemeng Zhou, Binlu Yu, Yuanjing Lin,* and Kwai Hei Li*



Cite This: *Nano Lett.* 2023, 23, 10674–10681



Read Online

ACCESS |

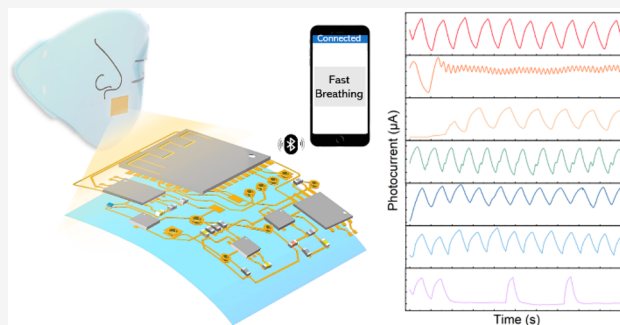
Metrics & More

Article Recommendations

Supporting Information

ABSTRACT: Respiratory pattern is one of the most crucial indicators for accessing human health, but there has been limited success in implementing fast-responsive, affordable, and miniaturized platforms with the capability for smart recognition. Herein, a fully integrated and flexible patch for wireless intelligent respiratory monitoring based on a lamellar porous film functionalized GaN optoelectronic chip with a desirable response to relative humidity (RH) variation is reported. The submillimeter-sized GaN device exhibits a high sensitivity of 13.2 nA/%RH at 2–70%RH and 61.5 nA/%RH at 70–90%RH, and a fast response/recovery time of 12.5 s/6 s. With the integration of a wireless data transmission module and the assistance of machine learning based on 1-D convolutional neural networks, seven breathing patterns are identified with an overall classification accuracy of >96%. This integrated and flexible on-mask sensing platform successfully demonstrates real-time and intelligent respiratory monitoring capability, showing great promise for practical healthcare applications.

KEYWORDS: Respiration sensors, lamellar porous films, GaN optoelectronic, 1-D CNNs



The respiration process, consisting of the breathing cycle of inhalation and exhalation, is considered to be one of the most important indicators for the early diagnosis of diseases and the assessment of human health. Recently, research on respiration monitoring and recognition has attracted growing interest since symptoms including sneezing, nasal congestion, and coughing can be the key potential signs of disease and inflection such as asthma and pulmonary hypertension.^{1,2} Various types of breathing detecting devices, such as capacitive,^{3–5} resistive,^{6–8} and optical,^{9–11} have been demonstrated to detect variations in pressure,^{12–15} temperature,^{15–18} and humidity^{19–22} introduced by human breathing. Among them, humidity sensing based on optical means is a promising candidate, which provides attractive features of noninvasive, rapid response, and high sensitivity. Current demonstrations of optical humidity sensing mostly involve the assembly and optical connection of external components, such as light sources, photodetectors, and light-guiding media,^{23–25} restricting their development toward miniaturization. Moreover, the integration of specified structures and coatings, such as hydrogel,²⁶ graphene,²⁷ and metal oxides,²⁸ is often required as sensitive media to perform effective humidity sensing.

To meet the rising demand for portable and wearable devices in healthcare applications,^{29–34} there is an urgent need to develop a humidity-sensing device with the features of compact size, quick response, facile integration, and inexpensive fabrication. On-chip integration of optoelectronic devices has garnered increasing attention. Notably, GaN-

based semiconductors are regarded as one of the most promising materials for developing optoelectronic devices due to their high efficiency, high stability, and long lifespan.^{35–37} Several devices based on GaN-based integrated devices have been proposed with prominent sensing capabilities including those for monitoring live-cell activities,³⁸ angle detection,³⁹ and salinity measurement.⁴⁰

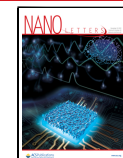
With the development and popularity of smart wearable devices, machine learning has received growing interest in the area of health and motion monitoring.⁴¹ In particular, the convolutional neural networks (CNNs)-assisted deep learning approach, which is structured as a series of convolutional layers and pooling operation, shows promise for improving the accuracy and reliability of processing complex signals such as physiological signals and complex human activities.⁴²

In this work, a fully integrated patch for wireless intelligent respiratory monitoring is proposed, and its schematic layout is shown in Figure 1a. The GaN optoelectronic chip with a size of 0.88 mm × 0.88 mm coated with a lamellar porous film is responsible for high-performance humidity sensing, as shown

Received: June 20, 2023

Revised: September 9, 2023

Published: September 15, 2023



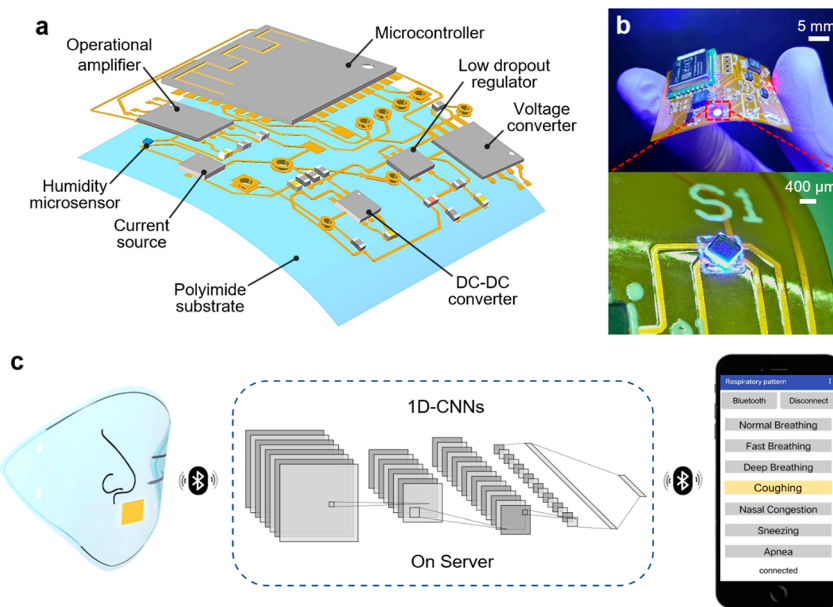


Figure 1. Configuration of the fully integrated patch. (a) Schematic diagram of the components on the PI PCB. (b) Optical image of the sensing patch and a magnified view showing the humidity-sensing device. (c) Schematic illustration of the operation of the patch for wireless intelligent respiratory monitoring.

in Figure 1b. The GaN device comprising a light emitter and light detector was monolithically integrated on the same chip through wafer-scale microfabrication processes. The low-cost lamellar porous film was coated on the surface of the device as a humidity-sensing medium, which is capable of producing optical changes according to humidity variation. The developed device together with custom-designed electronic modules was integrated on a polyimide (PI) printed circuit board (PCB) with a size of $33\text{ mm} \times 31\text{ mm}$, which enabled respiratory signal acquisition in a wireless manner. The transmitted signals were analyzed by 1-D CNNs to achieve the intelligent recognition of breathing patterns. Figure 1c depicts the operation of the patch for in-mask respiratory monitoring. Through wireless data transmission, the breathing signals were processed by the server, and the analyzed results were received by the mobile end.

Properties of GaN Optoelectronic Chip. The diode optopairs containing InGaN/GaN multiquantum wells (MQWs) function as light emitters and detectors. As schematically illustrated in Figure 2a, through current injection, the emitter emits light (wavelength peak = 455 nm, full-width at half-maximum = 22 nm) as a result of the carrier recombination in the MQW.^{43,44} The lamellar porous film establishes optical reflectance change based on humidity changes, thus varying the amount of light received by the detector. The reflected light is received by the MQWs of the detector to form electron–hole pairs, thereby generating photocurrents.

The electrical and optical properties of the diode pairs were investigated. The I – V curve of the emitter in Figure 2b shows a forward-biased voltage of 2.66 V at 10 mA and the resistance determined from the reciprocal slope of the linear region is $19.8\ \Omega$. The inset in Figure 2b indicates that the light output power of the emitter is linearly proportional to the bias current. As plotted in Figure 2c, under ambient lighting conditions with an illuminance of around 500 lx, the photocurrent of the detector measured under reverse bias voltage remains at a low level of the order of 10^{-9} A . When a constant current of

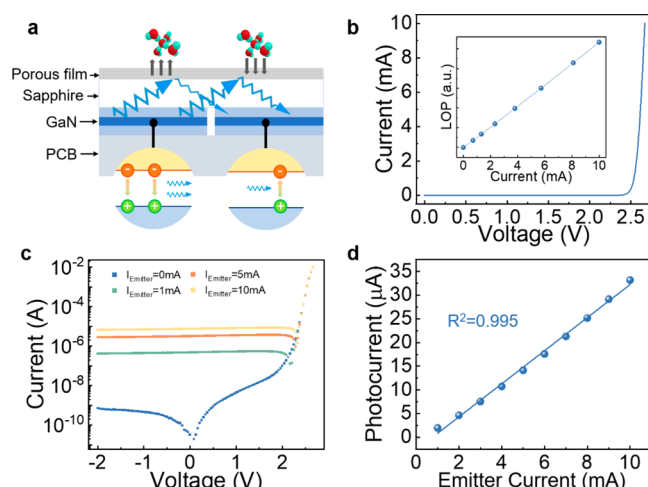


Figure 2. Humidity sensing principle and performance of the GaN device. (a) Schematic diagram of the working principle of the humidity sensor. (b) I – V curve of the light emitter. The inset shows the driving current–light optical power (LOP) curve of the light emitter. (c) I – V curve of the detector under different emitter currents. (d) Plot of the emitter current versus the detector photocurrent.

10 mA is applied to the emitter, the photocurrent rises to orders of magnitude of 10^{-5} A . The stable photocurrent with increasing reversed biased voltage suggests that the device leakage current is negligible. Figure 2d reveals a linear relationship between the photocurrent of the detector and the driving current of the emitter.

Characterization of the Porous Composite Film. The lamellar porous film plays an essential role in the humidity-sensing interface. The surface morphology was analyzed by scanning electron microscopy (SEM). The SEM image in Figure 3a shows the film coated on the device surface uniformly, and the thickness of the film is around $12\ \mu\text{m}$ (provided in Supporting Information S1). The porous

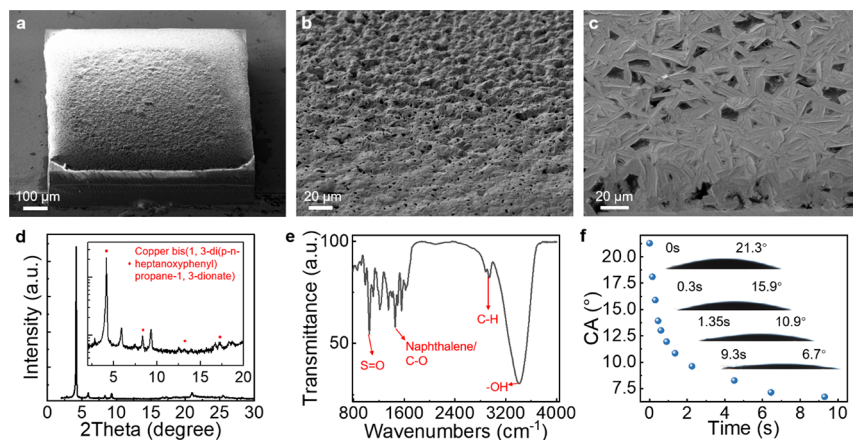


Figure 3. Characterizations of the lamellar porous film. (a) 45° tilted view SEM image of the coverage of the film on the device. (b) 45° tilted view and (c) cross-sectional view SEM images showing the film morphology. (d) XRD pattern of the film. Inset shows the same plot in a semilog scale. (e) FTIR pattern of the film. (f) Plot of contact angle versus time. Insets show the contact angles of the water droplets at different times.

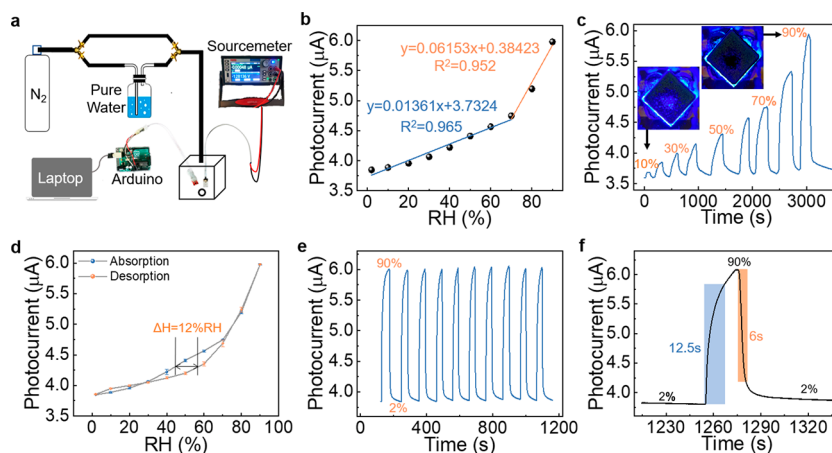


Figure 4. Characterizations of the device response to humidity change. (a) Schematic diagram of the experimental setup for humidity measurement. (b) Photocurrent response measured under different RH. (c) Dynamic response curve of 10–90%RH. Insets show the optical images of the operating device captured at low and high RH. (d) Hysteresis curve. (e) Repeatability test curve. (f) Transient response of the device. The blue and orange shaded areas represent the response time and recovery time based on the T90 method, respectively.

structure of the film can be clearly observed in the magnified SEM images shown in Figure 3b and c.

Copper coordination compounds are commonly used in printing inks,⁴⁵ which are the predominant components in the as-prepared lamellar porous film (see the SEM-EDS results in Supporting Information S2). As shown in Figure 3d, X-ray diffraction (XRD) analysis produces a pattern with main phases matches with copper bis(1,3di(p-n-heptanoxyphenyl)-propane-a,3-dionate). The functional groups of the copper coordination compounds are further confirmed by Fourier transform infrared (FTIR) results in Figure 3e. The spectrum of the ligand displays the characteristic S=O vibrations that are associated with the stretching vibrations of the SO₃ group at 1204 and 1018 cm⁻¹, respectively.⁴⁵ The band at 1621 cm⁻¹ is attributed to benzene ring stretching, and the one at 1558 cm⁻¹ is attributed to vibrations involving a combination of naphthalene ring and ν(CO) stretching.⁴⁶ A series of bands between 2700 and 3000 cm⁻¹ are the results of ν(CH) vibrations.⁴⁶ The strong broad band centered at 3400 cm⁻¹ with a broad shoulder at 3200 cm⁻¹ is attributed to ν(OH).⁴⁶ It is worth mentioning that the abundant hydrophilic functional groups in the film enable a highly sensitive response. Besides, reports on similar copper coordination compounds

also show lamellar and columnar morphologies,⁴⁷ which is consistent with the SEM characterization of the as-prepared porous composite film. It is believed that the copper coordination compounds in porous lamellar structure facilitate the desorption of water molecules that contributes to rapid recovery.⁴⁸

The wettability of the coated film was studied by measuring the contact angle of the water droplet. As shown in Figure 3f, the contact angle decreases exponentially with time. The figure insets further show the morphological changes in the contact angle of the water droplet. When the time is increased from 0 to 9.3 s, the contact angle decreases from 21.3° to 6.7°. The contact angles measured at different times are found to be less than 90°, implying that the film with hydrophilic properties is capable of rapid absorption of the water molecules.^{49,50}

Characterization of the Humidity-Sensing Device. The humidity sensing performance of the device was systematically studied. To measure the sensitivity of the as-fabricated device, the commercial SHT31 humidity sensor was used for comparison and the experimental setup was illustrated in Figure 4a. For the measurement of results shown in Figure 4b–f, the emitter was driven with a constant current of 10 mA and the detector remained unbiased. The photocurrent signals

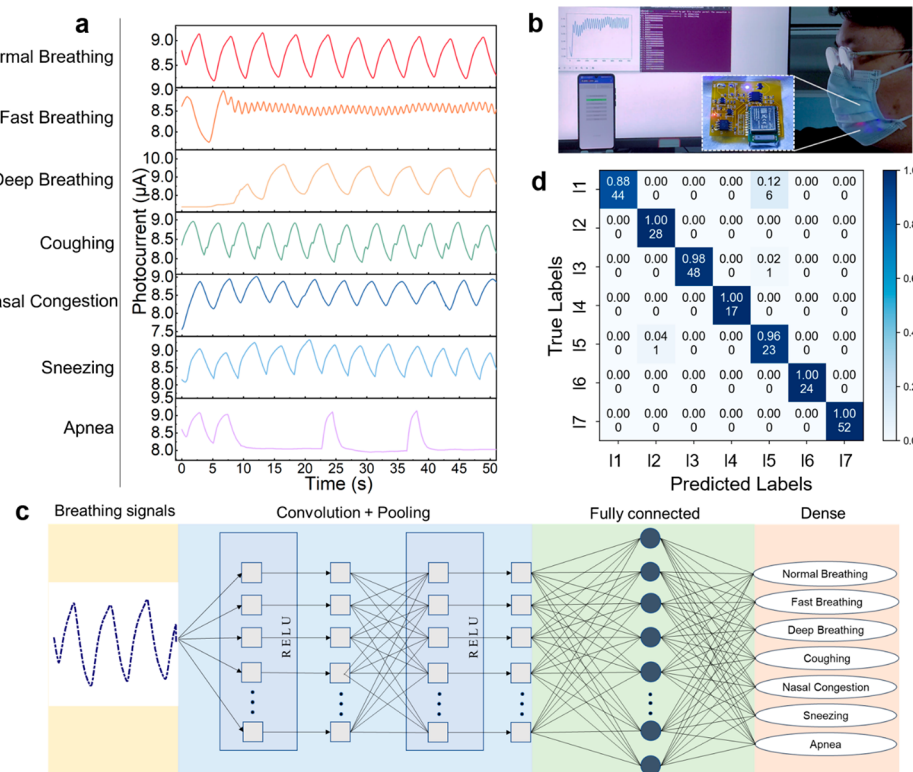


Figure 5. Recognition of breathing patterns. (a) Photocurrent waveforms measured under seven different breathing conditions. (b) Optical image showing the operation of the wireless humidity sensing patch. (c) Schematic diagram of the basic structure of 1-D CNNs. (d) Plot of the confusion matrix of seven breathing patterns (I1, I2, I3, I4, I5, I6, and I7, representing normal breathing, fast breathing, deep breathing, coughing, nasal congestion, sneezing, and apnea, respectively).

under relative humidity (RH) variation were acquired and are plotted in Figure 4b. The measured photocurrent increased monotonically as RH increased over a wide range of 2–90 RH %. The lamellar porous film exhibited a decrease in refractive index when RH increased, which caused a reduction in reflectance that matched the emission of the emitter (*Supporting Information S3*). Moreover, the hydrophilic nature of the film facilitated the rapid exchange of water molecules, and the adsorption of water molecules by the film exhibited rapid optical changes detected by the detector. By performing the linear fitting to the data in the two RH ranges of 2–70%RH and 70–90% RH, the sensitivities defined as $\Delta I/\Delta RH$ were 13.2 nA/%RH and 61.5 nA/%RH, respectively, where ΔRH was the RH difference and ΔI was the photocurrent difference. The higher sensitivity observed at high humidity compared to low humidity is due to the film introducing a more pronounced reflectance change in the range from 70%RH to 90% RH than in the range below 70% RH (see *Supporting Information S3*).

To study the continuous real-time monitoring capability, a dynamic response measurement of the device was carried out. Figure 4c shows the stepwise response curve of the device. As RH rises from 10%RH to 90%RH in a step of 10%RH, the photocurrent of the device rapidly increases to the targeted levels, indicating that the device had a good dynamic response in a wide RH range. The inset in Figure 4c further confirms that the amount of light transmitted through the film decreased as RH increased, which was consistent with the aforementioned reflectance characteristics. The device was further characterized under adsorption from 2 to 90%RH and desorption from 90 to 2%RH. From the curves plotted in

Figure 4d, the device had a hysteresis of about 12% at 50%RH. The repeatability of the photocurrent response was measured under humidity changes of 2–90%RH. Figure 4e indicates that the device had good repeatability over ten cycles. Figure 4f plots the response curve measured at RH between 2 and 90%. The response time and recovery time, defined as the time required for the sensor to reach 90% of the final stable reading, were determined to be around 12.5 and 6.0 s, respectively. Compared with the previously reported humidity-sensing devices that employed different mechanisms, the as-fabricated one exhibited superior performance in terms of wide measurement range and rapid response time (see *Supporting Information S4*). More importantly, the compact configuration of a submillimeter size enables the device to be readily integrated with wireless data transfer systems.

Machine Learning for Breathing Pattern Recognition.

After the device was characterized, its high sensitivity at high RH and fast response were the key features to enable monitoring of the human breathing pattern. In particular, the device can effectively detect breathing signals from a person wearing a mask in a high-humidity environment of 70–90% RH (see *Supporting Information S5*). Having considerable bending capability (*Supporting Information S6*), the sensing patch was fixed inside the facemask using 3M double-sided tape, and the breathing patterns generated by humans were acquired in a laboratory at room temperature and a humidity range of 50–60%RH. Apart from the results of different breathing rates and depths, abnormal states of apnea, sneezing, coughing, and nasal congestion can be detected, as shown in Figure 5a. Clinically, respiratory rate is generally defined as the times of respiration observed in 1 min, and its abnormality is

Table 1. Comparison of Smart Respiratory Monitoring Systems Based on Different Principles

Mechanism/material	Device size	Response/recovery time	Wired/wireless	Method/number of recognition pattern	Ref
Triboelectric/(a-PVDF/Epoxy)	15 mm × 15 mm	0.28 s (4 kPa, 1 Hz)	Wired	CNN, 5	54
Resistance/(ZnO/RGO)	13 mm × 7 mm	2/11 s (11–95% RH)	Wired	Waveform, 3	55
Resistance/Ni–Co–P HNBs	12 mm × 8 mm	95/27 s (9.05–97.5%RH)	Wired	Waveform, 3	56
TENG/CDs	N/A	N/A (11–94% RH)	Wired	Waveform, 3	57
Piezoelectric/AgOriPVDF	15 mm × 25 mm	N/A	Wired	Waveform, 3	58
Resistance/GO-NH ₂ /mSiO ₂	N/A	12.6/58.5 s (43–97% RH)	Wired	Waveform, 6	59
Temperature/Pt	R = 8 mm	N/A	Wireless	Waveform, 5	60
Optoelectronics//(GaN/composite film)	0.88 mm × 0.88 mm	12.5/6 s (10–90% RH)	Wireless	CNN, 7	This work

an important indicator of a serious clinical event such as hypoxemia, hypercarbia, anesthesia, and so on.⁵¹ Also, the prevalence of obstructive sleep apnea is as high as 40% to 80% among patients with cardiovascular disease.⁵² Acute upper respiratory tract viral infections (URTIs) are the most common diseases in humans; they may occur without symptoms, may be fatal, or are most commonly associated with an acute self-limiting illness. Sneezing is an early symptom of URTIs that appears and disappears quickly, while nasal congestion and cough are later symptoms of URTIs that appear slowly and persist for a long time.⁵³ The breathing signals transmitted wirelessly were processed by the server, and the analyzed results were sent to the mobile end, as shown in Figure 5b. Figure 5c illustrates the basic structure of 1-D CNNs for recognizing breathing patterns. Furthermore, a 3-fold cross-validation approach was employed to evaluate the performance of the network. Considering that the longest duration of one apnea cycle is around 14 s and each set includes at least one breathing pattern cycle, a total of 960 sets of data (each set including 700 points) for the seven breathing modes were collected at a sampling frequency of 50 Hz. Due to the influence of motion and variation of environmental RH, there was baseline drift with frequencies varying between 0.05 and 2 Hz. A Butterworth low-pass filter with a cutoff frequency of 5 Hz was utilized to eliminate the baseline interference (see Supporting Information S7). Then the breathing signals were normalized through the function of

$$\bar{x}_i = \frac{x_i - \mu}{\sigma} \quad (1)$$

where x_i and \bar{x}_i are the original signal and normalized result of each batch, respectively, while μ and σ represent the mean and standard deviation, respectively. This can accelerate the convergence rate of the model and reduce overfitting.

From the plot of the confusion matrix shown in Figure 5d, the overall accuracy can reach 96.72%. The convergence results of the model are shown in Supporting Information S7. The model classifications of deep breathing, fast breathing, coughing, sneezing, and apnea attained an accuracy of close to 100%. The demonstration of recognition of seven breathing patterns is provided in the Supporting Information. It is noted that the identification of normal breathing was shown to be less accurate due to the fact that it has a highly similar waveform to nasal congestion, while the major difference between them is peak-to-peak value. Compared with the intelligent respiratory monitoring systems reported in the literature, the sensing patch developed in this work provides outstanding features of small size, fast response, wireless operation, and the ability to recognize up to seven breathing patterns, as shown in Table 1.

Experimental Section/Methods. *Fabrication of the Humidity-Sensing Device.* The epitaxial structure containing an unintentionally doped GaN layer, Si-doped n-type GaN, InGaN/GaN MQWs, and Mg-doped p-type GaN was grown on 4 in. c-plane sapphire by metal–organic chemical vapor deposition. An indium tin oxide layer with a thickness of 120 nm was deposited on the surface of p-GaN as a current spreading layer. The mesas of diode pairs are formed by photolithography and inductively coupled plasma etching. A SiO₂ passivation layer is deposited by plasma-enhanced chemical vapor deposition, followed by the deposition of a SiO₂/TiO₂ distributed Bragg reflection layer using an optical thin-film coater. The p- and n-type electrodes were formed by photolithography, electron beam evaporation, and lift-off processes. The processed wafer is laser-diced into small chips with a size of 0.88 mm × 0.88 mm. Detailed descriptions of the process flow are provided in Supporting Information S8. The low-cost ink solution (HERO noncarbon ink 201) was treated in an ultrasonic water bath for 5 min and dropped onto the sapphire surface of the GaN device. After drying at room temperature for 30 min, a porous film is formed uniformly on the device surface. The GaN device integrated with the film constituted the resultant humidity-sensing device. It is worth noting that the response of bare GaN devices to humidity variations is highly limited. To achieve high sensitivity and fast response of the device to humidity changes, a moderate volume of 0.3 μL was chosen to ensure that the device was completely covered by the film (see Supporting Information S9).

Characterizations of the Device. The humidity in the test chamber was regulated by controlling the flow ratio of the drying air and humidified air. Nitrogen was used for dry air, and the humidified air was a bubbling system in which nitrogen was added to heated deionized water. The commercial SHT31 humidity sensing unit was together with the device in the test chamber for humidity calibration. The Keithley 2450 sourcemeter with a resolution of 50 pA was used to acquire photocurrent signals under varying RHs.

Design of the Wireless Data Transmission System. The system contained an NRF52840 microcontroller with analogue circuitry for signal conditioning, processing, and wireless transmission (see Supporting Information S10). TH1A10120 was used to generate a constant current of 10 mA to drive the device. LT1462CS8 amplifier cooperated with the resistor to form a transimpedance amplifier, which converts the photocurrent signals of the on-chip device into voltage signals. The voltage signal was acquired by a microcontroller with a built-in 12-bit analog-to-digital converter module and transmitted to a server through a Bluetooth low-energy (BLE) transceiver for signal processing. A low-power wireless system on chip

(NRF52840) with a 2.4 GHz transceiver was used to support the BLE protocols. A lithium-ion polymer battery (21 mm × 14 mm × 4 mm) with a capacity of 90 mAh at 3.7 V was used to drive the circuit. All electronic components were packaged on a PI PCB with a size of 33 mm × 31 mm.

In summary, a miniaturized wireless patch for intelligent respiration analysis is demonstrated. The humidity-sensing device is developed by integrating the GaN-based optoelectronic chip with the lamellar porous film. The hydrophilicity of the coated film facilitates the rapid exchange of water molecules, and the adsorption and desorption of water molecules effectively introduce the optical change of the film detectable by the on-chip detector. The device is packaged with wireless data transmission modules on a flexible PCB and demonstrates the ability to monitor human respiration. By applying machine learning based on 1-D CNNs on the collected signals, the recognition of seven breathing patterns with an overall classification accuracy of >96% is achieved. Owing to its fully integrated design, smart analysis, and wireless operation, the proposed sensing patch has considerable potential for health monitoring in various practical applications.

■ ASSOCIATED CONTENT

SI Supporting Information

The Supporting Information is available free of charge at <https://pubs.acs.org/doi/10.1021/acs.nanolett.3c02071>.

SEM images of cross-section view of lamellar porous film, SEM-EDS test of lamellar porous film, optical properties of lamellar porous film, comparison of humidity sensors, capability of the device to monitor human breathing patterns, bending characteristics of sensing patch, results of removing baseline drift and model convergence, fabrication procedure of the GaN device, deposition of the lamellar porous films on GaN devices, and design of wireless data transmission circuit ([PDF](#))

Demonstration of breathing pattern recognition ([MP4](#))

■ AUTHOR INFORMATION

Corresponding Authors

Kwai Hei Li – School of Microelectronics, Southern University of Science and Technology, Shenzhen 518055, P.R. China;
 orcid.org/0000-0002-0520-1632; Email: khli@sustech.edu.cn

Yuanjing Lin – School of Microelectronics, Southern University of Science and Technology, Shenzhen 518055, P.R. China;
 orcid.org/0000-0002-8568-1786; Email: linyj2020@sustech.edu.cn

Authors

Zecong Liu – School of Microelectronics, Southern University of Science and Technology, Shenzhen 518055, P.R. China

Junjie Su – School of Microelectronics, Southern University of Science and Technology, Shenzhen 518055, P.R. China

Kemeng Zhou – School of Microelectronics, Southern University of Science and Technology, Shenzhen 518055, P.R. China

Binlu Yu – School of Microelectronics, Southern University of Science and Technology, Shenzhen 518055, P.R. China

Complete contact information is available at:

<https://pubs.acs.org/doi/10.1021/acs.nanolett.3c02071>

Author Contributions

[†]Zecong Liu and Junjie Su contributed equally to this work.

Notes

The authors declare no competing financial interest.

■ ACKNOWLEDGMENTS

This work was supported by the National Natural Science Foundation of China (62201243, 62004088, and 12074170), the Shenzhen Natural Science Foundation Stability Support Program Project (20220815153728002), the Shenzhen Fundamental Research Program (JCYJ20220530113201003), and Southern University of Science and Technology Grant (Y01796108). The authors would like to acknowledge the technical support from SUSTech CRF.

■ REFERENCES

- (1) Dinh, T. N.; Nguyen, T. V.; Phan, H. P.; Nguyen, N. T.; Dao, D. V.; Bell, J. Stretchable Respiration Sensors: Advanced Designs and Multifunctional Platforms for Wearable Physiological Monitoring. *Biosens. Bioelectron.* **2020**, *166*, 112460.
- (2) Duan, Z.; Jiang, Y.; Tai, H. Recent Advances in Humidity Sensor for Human Body Related Humidity Detections. *Journal of Materials Chemistry C* **2021**, *9*, 14963–14980.
- (3) Lan, L.; Le, X.; Dong, H.; Xie, J.; Ying, Y.; Ping, J. One-Step and Large-Scale Fabrication of Flexible and Wearable Humidity Sensor Based on Laser-Induced Graphene for Real-Time Tracking of Plant Transpiration at Bio-Interface. *Biosens. Bioelectron.* **2020**, *165*, 112360.
- (4) Rauf, S.; Vijayap, M. T.; Andres, M. A.; Gascon, I.; Roubeau, O.; Eddaoudi, M.; Salama, K. N. Highly Selective Metal-Organic Framework Textile Humidity Sensor. *ACS Appl. Mater. Interfaces* **2020**, *12*, 29999–30006.
- (5) Chen, G.; Guan, R.; Shi, M.; Dai, X.; Li, H.; Zhou, N.; Chen, D.; Mao, H. A Nanoforest-Based Humidity Sensor for Respiration Monitoring. *Microsyst Nanoeng* **2022**, *8*, 44.
- (6) Duan, Z.; Zhao, Q.; Wang, S.; Huang, Q.; Yuan, Z.; Zhang, Y.; Jiang, Y.; Tai, H. Halloysite Nanotubes: Natural, Environmental-Friendly and Low-Cost Nanomaterials for High-Performance Humidity Sensor. *Sens. Actuators, B* **2020**, *317*, 128204.
- (7) Jeong, W.; Song, J.; Bae, J.; Nandanapalli, K. R.; Lee, S. Breathable Nanomesh Humidity Sensor for Real-Time Skin Humidity Monitoring. *ACS Appl. Mater. Interfaces* **2019**, *11*, 44758–44763.
- (8) Wu, J.; Sun, Y. M.; Wu, Z.; Li, X.; Wang, N.; Tao, K.; Wang, G. P. Carbon Nanocoil-Based Fast-Response and Flexible Humidity Sensor for Multifunctional Applications. *ACS Appl. Mater. Interfaces* **2019**, *11*, 4242–4251.
- (9) Chen, M.; Xue, S.; Liu, L.; Li, Z.; Wang, H.; Tan, C.; Yang, J.; Hu, X.; Jiang, X.-F.; Cheng, Y.; et al. A Highly Stable Optical Humidity Sensor. *Sens. Actuators, B* **2019**, *287*, 329–337.
- (10) Jang, J.; Kang, K.; Raeis-Hosseini, N.; Ismukhanova, A.; Jeong, H.; Jung, C.; Kim, B.; Lee, J. Y.; Park, I.; Rho, J. Self-Powered Humidity Sensor Using Chitosan-Based Plasmonic Metal–Hydrogel–Metal Filters. *Advanced Optical Materials* **2020**, *8*, 1901932.
- (11) Zhang, M.; Liu, Z.; Zhang, Y.; Zhang, Y.; Yang, X.; Zhang, J.; Yang, J.; Yuan, L. Spider Dragline Silk-Based Fp Humidity Sensor with Ultra-High Sensitivity. *Sens. Actuators, B* **2022**, *350*, 130895.
- (12) Zhong, J.; Li, Z.; Takakuwa, M.; Inoue, D.; Hashizume, D.; Jiang, Z.; Shi, Y.; Ou, L.; Nayyem, M. O. G.; Umez, S.; et al. Smart Face Mask Based on an Ultrathin Pressure Sensor for Wireless Monitoring of Breath Conditions. *Adv. Mater.* **2022**, *34*, No. e2107758.
- (13) Ghosh, R.; Song, M. S.; Park, J.; Tchoe, Y.; Guha, P.; Lee, W.; Lim, Y.; Kim, B.; Kim, S.-W.; Kim, M.; et al. Fabrication of Piezoresistive Si Nanorod-Based Pressure Sensor Arrays: A Promising Candidate for Portable Breath Monitoring Devices. *Nano Energy* **2021**, *80*, 105537.

- (14) Park, S. W.; Das, P. S.; Chhetry, A.; Park, J. Y. A Flexible Capacitive Pressure Sensor for Wearable Respiration Monitoring System. *IEEE Sensors Journal* **2017**, 1–1.
- (15) Pang, Z.; Zhao, Y.; Luo, N.; Chen, D.; Chen, M. Flexible Pressure and Temperature Dual-Mode Sensor Based on Buckling Carbon Nanofibers for Respiration Pattern Recognition. *Sci. Rep.* **2022**, 12, 17434.
- (16) Shin, J.; Jeong, B.; Kim, J.; Nam, V. B.; Yoon, Y.; Jung, J.; Hong, S.; Lee, H.; Eom, H.; Yeo, J.; et al. Sensitive Wearable Temperature Sensor with Seamless Monolithic Integration. *Adv. Mater.* **2020**, 32, No. e1905527.
- (17) Chen, S.; Qian, G.; Ghanem, B.; Wang, Y.; Shu, Z.; Zhao, X.; Yang, L.; Liao, X.; Zheng, Y. Quantitative and Real-Time Evaluation of Human Respiration Signals with a Shape-Conformal Wireless Sensing System. *Adv. Sci. (Weinh)* **2022**, 9, No. e2203460.
- (18) Chen, J.; Wang, F.; Zhu, G.; Wang, C.; Cui, X.; Xi, M.; Chang, X.; Zhu, Y. Breathable Strain/Temperature Sensor Based on Fibrous Networks of Ionogels Capable of Monitoring Human Motion, Respiration, and Proximity. *ACS Appl. Mater. Interfaces* **2021**, 13, 51567–51577.
- (19) Wang, Y.; Zhang, L.; Zhang, Z.; Sun, P.; Chen, H. High-Sensitivity Wearable and Flexible Humidity Sensor Based on Graphene Oxide/Non-Woven Fabric for Respiration Monitoring. *Langmuir* **2020**, 36, 9443–9448.
- (20) Su, Y.; Li, C.; Li, M.; Li, H.; Xu, S.; Qian, L.; Yang, B. Surface Acoustic Wave Humidity Sensor Based on Three-Dimensional Architecture Graphene/Pva/Sio₂ and Its Application for Respiration Monitoring. *Sens. Actuators, B* **2020**, 308, 127693.
- (21) Li, Z.; Teng, M.; Yang, R.; Lin, F.; Fu, Y.; Lin, W.; Zheng, J.; Zhong, X.; Chen, X.; Yang, B.; et al. Sb-Doped Wo₃ Based Qcm Humidity Sensor with Self-Recovery Ability for Real-Time Monitoring of Respiration and Wound. *Sens. Actuators, B* **2022**, 361, 131691.
- (22) Xing, H.; Li, X.; Lu, Y.; Wu, Y.; He, Y.; Chen, Q.; Liu, Q.; Han, R. P. S. Mxene/Mwcnt Electronic Fabric with Enhanced Mechanical Robustness on Humidity Sensing for Real-Time Respiration Monitoring. *Sens. Actuators, B* **2022**, 361, 131704.
- (23) Menon, S.; Usha, S. P.; Manoharan, H.; Kishore, P. V. N.; Sai, V. V. R. Metal-Organic Framework-Based Fiber Optic Sensor for Chromium(Vi) Detection. *ACS Sens* **2023**, 8, 684–693.
- (24) Fay, C. D.; Nattestad, A. Advances in Optical Based Turbidity Sensing Using Led Photometry (Pedd). *Sensors (Basel)* **2022**, 22, 254.
- (25) Chen, M.-q.; Zhao, Y.; Wei, H.-m.; Zhu, C.-l.; Krishnaswamy, S. 3d Printed Castle Style Fabry-Perot Microcavity on Optical Fiber Tip as a Highly Sensitive Humidity Sensor. *Sens. Actuators, B* **2021**, 328, 128981.
- (26) Wu, Z.; Ding, Q.; Li, Z.; Zhou, Z.; Luo, L.; Tao, K.; Xie, X.; Wu, J. Ultrasensitive, Stretchable, and Transparent Humidity Sensor Based on Ion-Conductive Double-Network Hydrogel Thin Films. *Science China Materials* **2022**, 65, 2540–2552.
- (27) Cai, J.; Lv, C.; Aoyagi, E.; Ogawa, S.; Watanabe, A. Laser Direct Writing of a High-Performance All-Graphene Humidity Sensor Working in a Novel Sensing Mode for Portable Electronics. *ACS Appl. Mater. Interfaces* **2018**, 10, 23987–23996.
- (28) Subki, A. S. R. A.; Mamat, M. H.; Manut, A.; Birowosuto, M. D.; Musa, M. Z.; Rusop, M. M. Composite Effect on Zinc Oxide Based Resistive Type Humidity Sensor Performance: A Preliminary Assessment. *Journal of Electrical & Electronic Systems Research* **2022**, 20, 18–28.
- (29) Zhao, J.; Lin, Y.; Wu, J.; Nyein, H. Y. Y.; Bariya, M.; Tai, L.-C.; Chao, M.; Ji, W.; Zhang, G.; Fan, Z.; et al. A Fully Integrated and Self-Powered Smartwatch for Continuous Sweat Glucose Monitoring. *ACS sensors* **2019**, 4, 1925–1933.
- (30) Lin, Y.; Bariya, M.; Nyein, H. Y. Y.; Kivimäki, L.; Uusitalo, S.; Jansson, E.; Ji, W.; Yuan, Z.; Happonen, T.; Liedert, C.; et al. Porous Enzymatic Membrane for Nanotextured Glucose Sweat Sensors with High Stability toward Reliable Noninvasive Health Monitoring. *Adv. Funct. Mater.* **2019**, 29, 1902521.
- (31) Fan, Z.; Chen, Y.; Lin, Y.; Zi, Y.; Ko, H.; Zhang, Q. Preface to the Special Issue on Flexible Energy Devices. *Journal of Semiconductors* **2021**, 42, 100101–100102.
- (32) Ma, X.; Jiang, Z.; Lin, Y. Flexible Energy Storage Devices for Wearable Bioelectronics. *Journal of Semiconductors* **2021**, 42, 101602.
- (33) Lin, Y.; Bariya, M.; Javey, A. Wearable Biosensors for Body Computing. *Adv. Funct. Mater.* **2021**, 31, 2008087.
- (34) Zeng, X.; Peng, R.; Fan, Z.; Lin, Y. Self-Powered and Wearable Biosensors for Healthcare. *Materials Today Energy* **2022**, 23, 100900.
- (35) Yan, J.; Piao, J.; Wang, Y. An Enhancement Mode Mosfet Based on Gan-on-Silicon Platform for Monolithic Oeic. *IEEE Electron Device Lett.* **2020**, 41, 76–79.
- (36) Li, Y.; Yang, Y.; Gao, X.; Yuan, J.; Zhu, G.; Zhang, Z.; Wang, Y. Light Induced Synaptic Transistor with Dual Operation Modes. *IEEE Electron Device Lett.* **2016**, 37, 1434–1437.
- (37) Li, K. H.; Fu, W. Y.; Choi, H. W. Chip-Scale Gan Integration. *Progress in Quantum Electronics* **2020**, 70, 100247.
- (38) Hou, Y.; Jing, J.; Luo, Y.; Xu, F.; Xie, W.; Ma, L.; Xia, X.; Wei, Q.; Lin, Y.; Li, K. H.; et al. A Versatile, Incubator-Compatible, Monolithic Gan Photonic Chipscope for Label-Free Monitoring of Live Cell Activities. *Advanced Science* **2022**, 9, 2200910.
- (39) Yin, J.; Yang, H.-Q.; Luo, Y.; Wang, Q.; Yu, H.; Li, K. H. Iii-Nitride Microsensors for 360° Angle Detection. *IEEE Electron Device Lett.* **2022**, 43, 458–461.
- (40) Jing, J.; Hou, Y.; Luo, Y.; Chen, L.; Ma, L.; Lin, Y.; Li, K. H.; Chu, Z. Chip-Scale In Situ Salinity Sensing Based on a Monolithic Optoelectronic Chip. *ACS sensors* **2022**, 7, 849–855.
- (41) Bokka, N.; Karhade, J.; Sahatiya, P. Deep Learning Enabled Classification of Real-Time Respiration Signals Acquired by Mosse Quantum Dot-Based Flexible Sensors. *Journal of materials chemistry. B* **2021**, 9 (34), 6870–6880.
- (42) Tang, K.; Kumar, A. G. B.; Nadeem, M.; Maaz, I. Cnn-Based Smart Sleep Posture Recognition System. *IoT* **2021**, 2, 119–139, DOI: 10.3390/iot2010007.
- (43) Li, K. H.; Cheung, Y. F.; Jin, W.; Fu, W. Y.; Lee, A. T. L.; Tan, S. C.; Hui, S. Y.; Choi, H. W. Ingan Rgb Light-Emitting Diodes with Monolithically Integrated Photodetectors for Stabilizing Color Chromaticity. *IEEE Transactions on Industrial Electronics* **2020**, 67, S154–S160.
- (44) Li, K. H.; Cheung, Y. F.; Fu, W. Y.; Wong, K. K.-Y.; Choi, H. W. Monolithic Integration of Gan-on-Sapphire Light-Emitting Diodes, Photodetectors, and Waveguides. *IEEE J. Sel. Top. Quantum Electron.* **2018**, 24, 1–6.
- (45) Elsawy, M. M.; Faheim, A. A.; Salem, S. S.; Owda, M. E.; Abd El-Wahab, Z. H.; Abd El-Wahab, H. Cu (Ii), Zn (Ii), and Ce (Iii) Metal Complexes as Antimicrobial Pigments for Surface Coating and Flexographic Ink. *Appl. Organomet. Chem.* **2021**, 35, No. e6196.
- (46) Dines, T. J.; Onoh, H. An Infrared and Resonance Raman Spectroscopic Study of Phenylazonaphthol Pigments. *Spectrochimica acta. Part A, Molecular and biomolecular spectroscopy* **2006**, 64, 891–900.
- (47) Usha, K.; Vijayan, K.; Sadashiva, B. K. Crystal and Molecular Structure of the Discogen Bis[1,3-Di(P-N-Octylphenyl)Propane-1,3-Dionato]Copper(Ii). *Mol. Cryst. Liq. Cryst.* **1989**, 201, 13–21.
- (48) Wang, L.; He, Y.; Hu, J.; Qi, Q.; Zhang, T. Dc Humidity Sensing Properties of Batio₃ Nanofiber Sensors with Different Electrode Materials. *Sensors and Actuators B-chemical* **2011**, 153, 460–464.
- (49) Yu, X.; Wang, Z.; Jiang, Y.; Shi, F.; Zhang, X. Reversible Ph-Responsive Surface: From Superhydrophobicity to Superhydrophilicity. *Adv. Mater.* **2005**, 17, 1289–1293.
- (50) Feng, X.; Feng, L.; Jin, M.; Zhai, J.; Jiang, L.; Zhu, D. Reversible Super-Hydrophobicity to Super-Hydrophilicity Transition of Aligned Zno Nanorod Films. *J. Am. Chem. Soc.* **2004**, 126, 62–63.
- (51) Liu, H.; Allen, J.; Zheng, D.; Chen, F. Recent Development of Respiratory Rate Measurement Technologies. *Physiological measurement* **2019**, 40, No. 07TR01.
- (52) Yeghiazarians, Y.; Jneid, H.; Tietjens, J. R.; Redline, S.; Brown, D. L.; El-Sherif, N.; Mehra, R.; Bozkurt, B.; Ndumele, C. E.; Somers,

V. K. Obstructive Sleep Apnea and Cardiovascular Disease: A Scientific Statement from the American Heart Association. *Circulation* **2021**, *144*, e56–e67.

(53) Eccles, R. Understanding the Symptoms of the Common Cold and Influenza. *Lancet infectious diseases* **2005**, *5*, 718–725.

(54) Fang, Y.; Xu, J.; Xiao, X.; Zou, Y.; Zhao, X.; Zhou, Y.; Chen, J. A Deep-Learning-Assisted on-Mask Sensor Network for Adaptive Respiratory Monitoring. *Adv. Mater.* **2022**, *34*, No. e2200252.

(55) Zhang, H.; Gu, W.; Chen, C. Preparation and Mechanism Analysis of Non-Contact Respiratory Sensor Based on ZnO/Rgo Composites. *Appl. Surf. Sci.* **2022**, *599*, 154031.

(56) Chen, C.; Jiang, M.; Luo, X.; Tai, H.; Jiang, Y.; Yang, M.; Xie, G.; Su, Y. Ni-Co-P Hollow Nanobricks Enabled Humidity Sensor for Respiratory Analysis and Human-Machine Interfacing. *Sens. Actuators, B* **2022**, *370*, 132441.

(57) Qin, J.; Yang, X.; Shen, C.; Chang, Y.; Deng, Y.; Zhang, Z.; Liu, H.; Lv, C.; Li, Y.; Zhang, C.; et al. Carbon Nanodot-Based Humidity Sensor for Self-Powered Respiratory Monitoring. *Nano Energy* **2022**, *101*, 107549.

(58) Jin, L.; Zheng, Y.; Liu, Z.; Li, J.; Zhai, H.; Chen, Z.; Li, Y. Design of an Ultrasensitive Flexible Bend Sensor Using a Silver-Doped Oriented Poly(Vinylidene Fluoride) Nanofiber Web for Respiratory Monitoring. *ACS Appl. Mater. Interfaces* **2020**, *12*, 1359–1367.

(59) Zhu, J.; Zhang, N.; Yin, Y.; Xu, B.; Zhang, W.; Wang, C. High-Sensitivity and Low-Hysteresis GO-NH₂/Mesoporous SiO₂ Nanosphere-Fabric-Based Humidity Sensor for Respiratory Monitoring and Noncontact Sensing. *Advanced Materials Interfaces* **2022**, *9*, 2101498.

(60) Cao, L.; Zhang, Z.; Li, J.; Wang, Z.; Ren, Y.; Wang, Q.; Huang, D.; Li, Z. A Low-Cost Flexible Perforated Respiratory Sensor Based on Platinum for Continuous Respiratory Monitoring. *Micromachines (Basel)* **2022**, *13*, 1743.